electrochem

MDPI

Article

Electric Field-Dependence of Double Layer Capacitances by Current-Controlled Charge-Discharge Steps

Ridong He [1], Koichi Jeremiah Aoki [2] and Jingyuan Chen [1,*]

[1] Department of Applied Physics, University of Fukui, 3-9-1 Bunkyo, Fukui 910-0017, Japan; heridong@yahoo.com
[2] Electrochemistry Museum, Fukui 910-0804, Japan; kaoki@u-fukui.ac.jp
* Correspondence: jchen@u-fukui.ac.jp

Received: 1 May 2020; Accepted: 5 June 2020; Published: 8 June 2020

Abstract: Voltage vs. time curves of double layer capacitances (DLCs) by current-controlled charge and discharge steps have been recognized to be composed of triangular waves. They are deviated slightly from triangles from the viewpoint of the time dependence or the constant phase element of the DLC. In order to evaluate the deviation, we measured DLCs of a platinum (Pt) electrode in KCl solution by current-control. Each time-voltage curve was convex rather a line, and was followed by the power law. Even if the time dependence was subtracted from each curve, the enhancement of the DLC was noticeable with an increase in the time well as the voltage. It can be attributed to the electric field effect, in which dipoles of solvents are oriented on an electrode so strongly that the DLC may be increased. The field dependence can be justified with the kinetic theory of interacting dipoles of solvents on an electrode through the observed linearity of the logarithmic DLC with the net voltage. This concept was applied to a commercially available super-capacitor to demonstrate a significant contribution of the field effect.

Keywords: electric field effects of double layer capacitance; enhancement of capacitance with voltage; constant phase elements; non-linear voltage-time curves; current-controlled charge and discharge

1. Introduction

A super-capacitor is a candidate back-up power supply because it can provide high current density in comparison with chemical batteries such as lithium ion batteries [1,2]. It belongs to a double layer capacitor (DLC) with a large net area of the electrode. The high current density [3] can be caused by physical processes of localization of charge, such as orientation of dipoles or heterogeneous distribution of ions rather than electrochemical reaction rates in chemical batteries. A question is what happens at extremely high current density. A voltage(V)–time(t) curve at constant current, I, through an ideal capacitance, C, should take a line segment, given by $V = (I/C)t$, according the definition of the capacitance, $C = q/V = It/V$ for the charge q in the sense of electromagnetics. However, experimentally charging curves are deviated from the linearity so that the slope of the tangent line gets small with an increase in voltage or the time [4]. The deviation has been ascribed to space charge effects [5], solution resistance [6,7], morphology of electrodes [8], charge of adsorbed species [9], distributed resistance and capacitance [10], participation in redox reactions [11,12], and frequency dispersion [13]. Although one of them may be a cause of the deviation, it is necessary to discuss the deviation quantitatively to search an attribution. A resistance involved in capacitive circuits cannot explain the deviation because it causes only a voltage shift. A capacitance generally exhibits time and voltage dependence [14–18], and hence a DLC was examined in detail.

The time dependence is equivalent to the frequency dispersion observed in ac-impedance measurements. The dispersion has been expressed quantitatively with constant phase elements [19–22] and the power law [23–26]. If the dispersion were to arise from the orientation period of dipoles of solvents or salts, it might take a time less than nano-seconds. The observed time scale as long as a second can be attributed to the cooperative phenomenon in which oriented dipoles take the minimum energy spread widely to a two-dimensional electrode by interaction [27]. The microscopic time scale is expanded to a macroscopic one, in accordance with the expansion of domains of the orientation. Since the power law has been derived from the thermodynamic viewpoint [28], it can be utilized for quantitative analysis of time-depending DLC.

An increase in the electric field (abbreviated as field) enhances the orientation of dipoles or capacitance values. Further increase in the field or the voltage causes irreversibly electrochemical decomposition of the capacitance. From the experimental viewpoint, the voltage dependence has been examined and explained in terms of variations of dielectrics of polymers [14,15], hopping conduction [16], time-dependent charge diffusion [17], and charge in orientation direction [18].

The present work deals with the time dependence and/or the voltage dependence of a DLC by applying constant currents to a platinum electrode in KCl solution. Our aim is to search how both kinds of the dependence are revealed in the charging and discharging curves in conventional voltammetry at platinum in KCl solution. Our prediction is the time dependence can be explained in terms of the power law, whereas the voltage dependence, which has not been well-known yet, will be revealed in the large voltage variation. The latter will be demonstrated theoretically from the kinetic theory of the power law. It is important industrially for designing supercapacitors because it varies the electric energy through $\int CV\mathrm{d}V/2$. Our discussion will be directed to the two kinds of the dependence from the physical viewpoint, which cover in principle properties of industrially applied capacitances [29].

2. Materials and Methods

A platinum wire 0.5 mm in diameter was used for a working electrode by inserting it into the aqueous KCl solution by a given length, ca. 8 mm. The accurate length was controlled with an optical Z-stage and was determined with an optical microscope. The electrode was not sealed with insulating materials, because the sealing often gives rise to floating capacitive current owing to imperfect boundaries between the electrode and the insulator. The counter electrode was a platinum wire with the area 100 times larger that of the working electrode, and the reference electrode was Ag|AgCl in saturated KCl solution. The test solution was deaerated for 20 min before the current application. An aqueous solution of KCl was prepared with the analytical grade of KCl to be 0.1 M and distilled and deionized water prepared by CPW-100 (Advantec, Tokyo, Japan). The potentiostat was Compactstat (Ivium, Eindhoven, The Netherlands) for chronopotentiometry and ac-impedance measurements. A supercapacitor was a commercially available (part number SE-5R5-D105VYV) with nominal values of 1 F capacitance, 5.5 V maximum voltage, and equivalent series resistance 22 Ω at 1 kHz (Tokin, Miyagi, Japan). All measurements were made at temperature of 25 ± 0.5 °C. Voltammetric reproducibility was examined at each experimental run. Reproducibility of our voltage-time curves was examined at three runs to be within 5% errors. Errors in the most graphs were close to the sizes of marks of the plots.

3. Results and Discussion

An example of iterative charge–discharge curves is shown in Figure 1A, where the constant current (0.7 μA) was applied to the Pt wire immersed into KCl solution for a second from the open circuit potential (0.21 V vs. Ag|AgCl) and then the current direction was reversed. The voltage, V, increased in the approximately linear form with the time for the charging step, but the detailed variation shows $\mathrm{d}^2V/\mathrm{d}t^2 < 0$. In contrast, the discharge step exhibits an approximately decreasing line very slightly with $\mathrm{d}^2V/\mathrm{d}t^2 > 0$. The voltage at $t = 3$ s at the discharging step was less than the initial voltage before the charging step ($t < 1$ s). Further iterative current control provided the iterative triangular current–time

responses. Our data analysis was limited to the curves less than 0.5 V at the risk of contribution of formation of platinum oxide [30] on the Pt electrode surface.

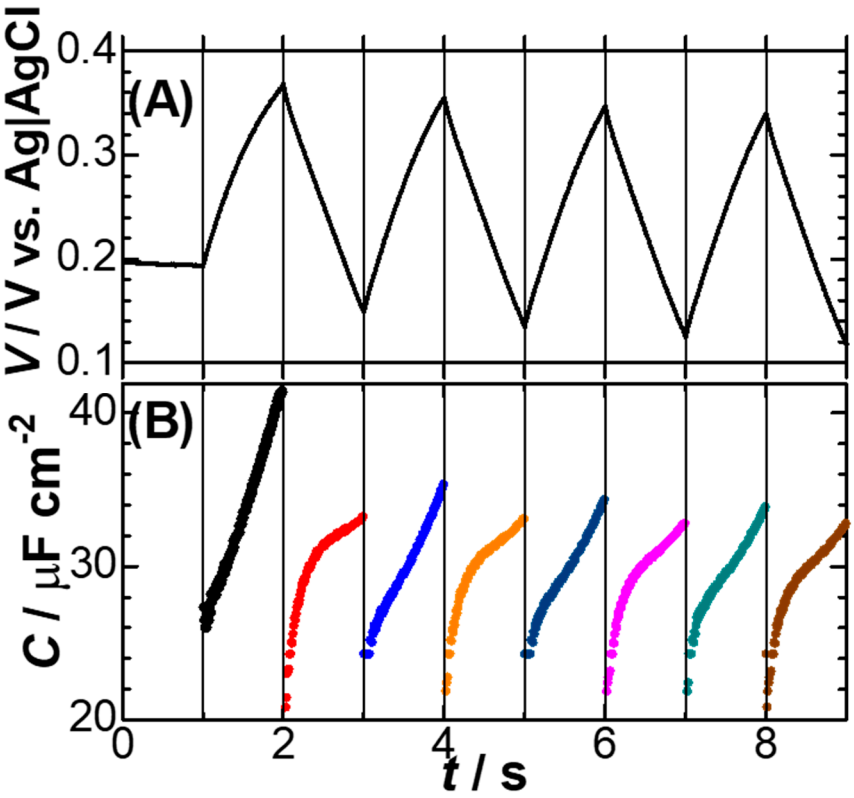

Figure 1. Voltage-time curves (**A**) responding to the iterative charge–discharge currents of ±0.7 μA at the Pt wire electrode in 0.1 M KCl aqueous solution, and the capacitance values (**B**) calculated from Equation (1). The direction of the current changed at each 1 s.

The deviation ($d^2V/dt^2 \neq 0$) from the lines in Figure 1A suggests the time dependence of the capacitance. According to the definition of the capacitance, $q = CV$ for a charge q in electromagnetics, the capacitance responding to a constant current is represented by

$$C = (j/|V - V_{in}|)t, \quad (1)$$

where j is the current density, and V_{in} is the initial voltage just after the reversal of the sign of the currents. Figure 1B shows dependence of C, thus, evaluated from Equation (1) on the time for the geometrical surface area of the immersed part of the wire, exhibiting an increasing function of t at each period. The time increase in C is in accordance with the frequency dispersion in which higher frequency decreases the capacitance by the power law [25,26]. By replacing the frequency by the time, we can write the law for a constant λ as [31],

$$C = C_{1s}t^{\lambda}, \quad (2)$$

where C_{1s} is the capacitance value at $t = 1$ s. We examined the validity of the power law by plotting log C against log($t - t_n$). Figure 2 shows the variations at each period, $t_n < t < t_{n+1}$, where t_n is the switching time of n seconds. The successive plots for $n = 3, 5, 7, \ldots$ of the charging step are overlapped, and those for $n = 2, 4, 6, \ldots$ of the discharging step also are. We discarded the wave at the first step ($n = 1$) because of dependence on the initial conditions. The deviation from a line can be recognized in both the charging and the discharging steps. The changing width of the voltage in Figure 1 was close to 0.2 V, which is much larger than ac-impedance method (0.01 V). The time dependence of C by the

ac-impedance [23–28] and chronoamperometry [31] did not deviate from Equation (1) except for an extremely short time. Consequently, the deviation from a line in Figure 2 may be caused by the voltage dependence observed when the voltage is large.

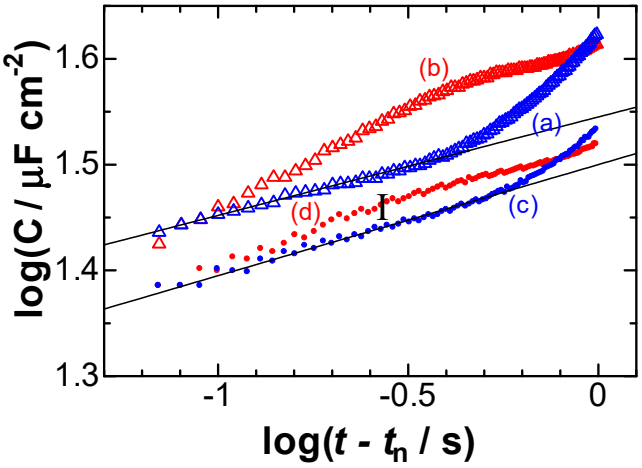

Figure 2. Time variations of the capacitance in the logarithmic scale for the (a, c, blue) charging (t_n = 3 s) and the (b, d, red) discharging (t_n = 4 s) steps at I = (a,b) 0.7 μA and (c,d) 1.5 μA. "I" means the error bar.

The short time variations in Figure 2 are expected to represent the time dependence rather than the voltage dependence because they are limited to a narrow voltage domain. The intercept of the line provides C_{1s}, whereas the slope of the line can be used for evaluating λ mentioned in Equation (2). These values for the short time at the charging step are plotted against the current in Figure 3. Values of λ are almost independent of the currents, indicating that C vs. t curves at short time in Figure 2 should be obeyed by the power law. In contrast, C_{1s} in Figure 3 has a linear relation to the current. The value at the intercept, ca. 30 μF cm^{-2}, is close to those by ac-impedance [23,25]. Since C_{1s} does not include the contribution of any time-variation, the linear relation in Figure 3 implies an effect of the voltage or the field. This effect can be deduced from the increase in the DLC obtained by ac-impedance with the ac-amplitude, V_{ac}, as shown in the inset of Figure 4. Unfortunately, it is difficult for us to evaluate accurately C_{1Hz} at large amplitude because of a loss of suitable theory [16].

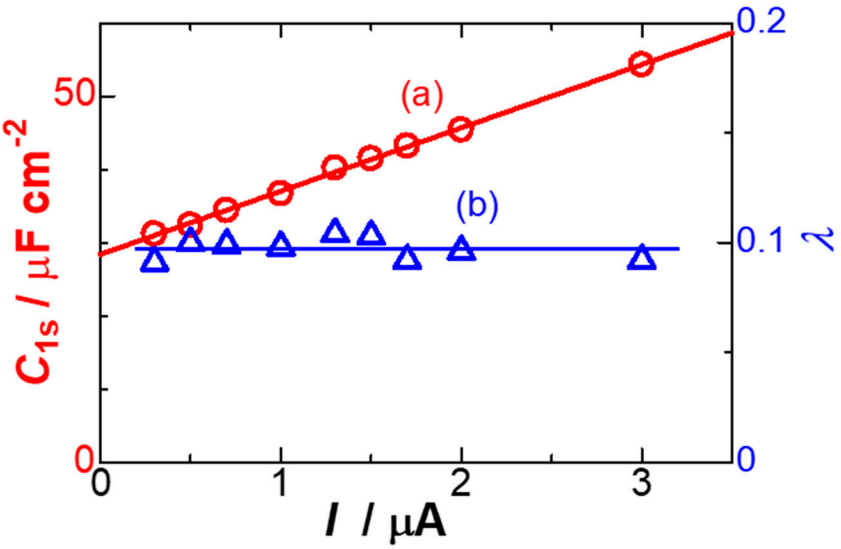

Figure 3. Variations of (a) C_{1s} and (b) λ with applied currents at the charging step.

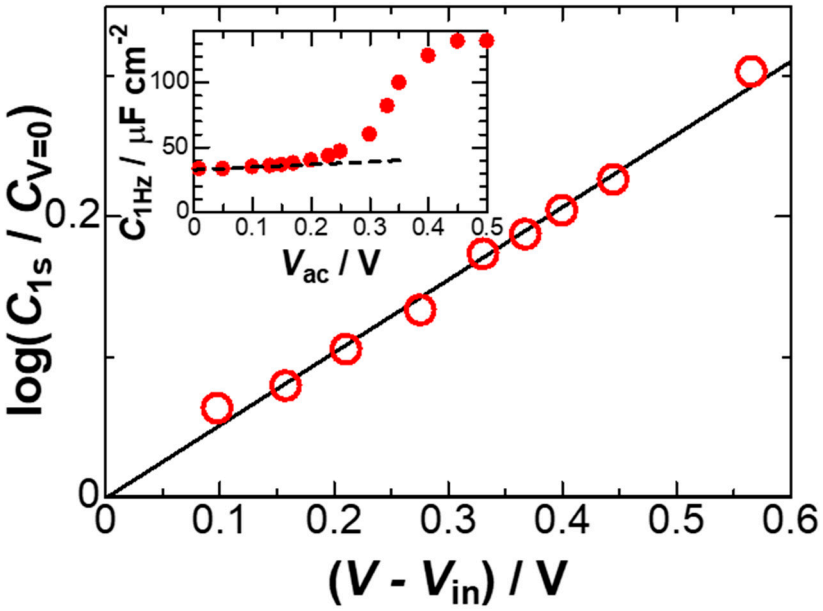

Figure 4. Logarithmic variation of $C_{1s}/C_{V=0}$ with the net voltage, $V - V_{in}$. The inset is the variation of the capacitance values determined by ac-impedance at several ac-amplitude, V_{ac}.

According to the theory of the power law [28], the time-dependent capacitance is approximated as

$$C = K \exp(-u_0/k_B T)\, t^{\lambda}, \tag{3}$$

where u_0 is the orientation energy of the dipole, k_B is the Boltzmann constant, and K is a proportional constant. By letting the dipole moment to be p, the orientation energy by the field E is given by $-pE$. If the field is applied to the dipole length, d, which can be estimated from the molar water molecule, the energy can be approximated as $u_0 = -pE = -p(V - V_{in})/d$. Taking the ratio to the capacitance $C_0 = Kt^{\lambda}$ at $V = V_{in}$ or $I = 0$, and taking the logarithm yields

$$\log(C/C_0) = p(V - V_{in})/2.3k_B Td, \tag{4}$$

Figure 4 shows a plot of $\log(C/C_0)$ of Figure 3 against $V - V_{in}$. The proportionality was found, for which the slope, $(p/2.3k_B Td)$, was 0.52 V^{-1}. This value allows us to determine p from $d = 0.31$ nm for the molar volume of water molecule. We obtained $p = 1.2 \times 10^{-30}$ Cm, which is 20% of the dipole moment of water molecule (6.1×10^{-30} Cm). The partial contribution of the orientation energy implies the contribution of the thermal fluctuation. Since the variable $p(V - V_{in})/d$ means energy, the exponential form in Equation (3) can be regarded as a kinetic equation for the DLC with the activation energy, $p(V - V_{in})/d$.

We apply the concept of the field dependence to a commercially available supercapacitor with 1 F and the permissible voltage domain 5.5 V. The voltage-time curves for an application of 0.1 A are shown in Figure 5A. Voltage skips by 1 V were found just after the change of the currents. They should be the cell resistance (10 Ω). Values of the capacitance calculated through Equation (1) are drawn in Figure 5B, where a 1 V ohmic drop was corrected. The measured values vary largely with the time and are smaller than the full capacitance value, 1 F. The variation can be ascribed to the time dependence and the voltage dependence of the supercapacitor. The plot of log C against $\log(t - t_n)$ exhibits a line with 0.6 (not shown here), which is much larger than the λ-value (0.1) in Figure 2. The extraordinarily large value cannot be attributed to the time dependence but should be to an alternative effect; i.e., the field effect. In fact, logarithmic values of C increase with an increase in $V - V_{in}$, as shown in Figure 6. The slope Figure 6(a) for small values of V-V_{in} is close to that in Figure 4. The smaller slopes at large values of $V - V_{in}$ may result from interaction of among oriented dipoles.

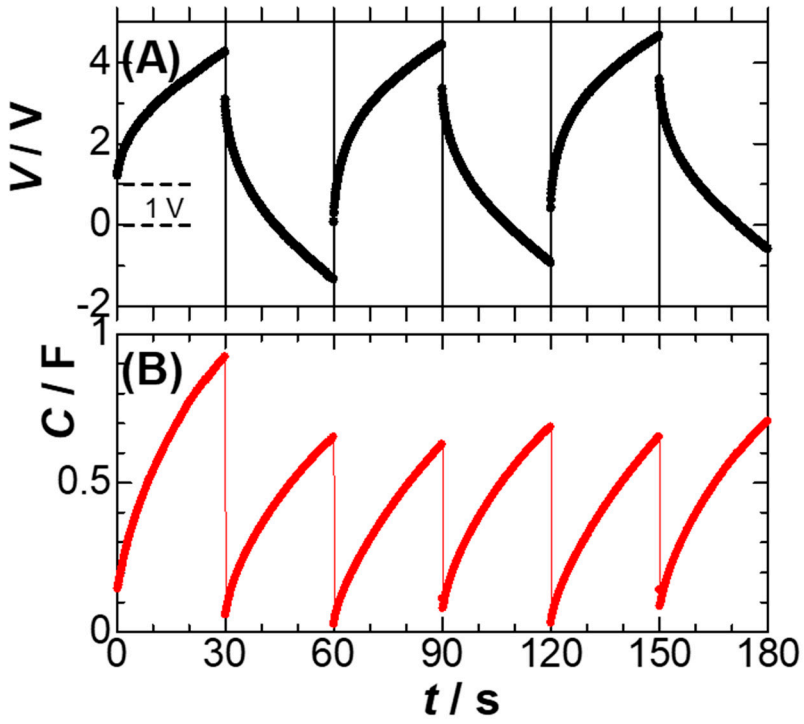

Figure 5. Voltage–time curves (**A**) responding to the iterative charge–discharge currents of ±0.1A at the 1 F super-capacitor, and the capacitance values (**B**) calculated from Equation (1) vary with the corresponding time.

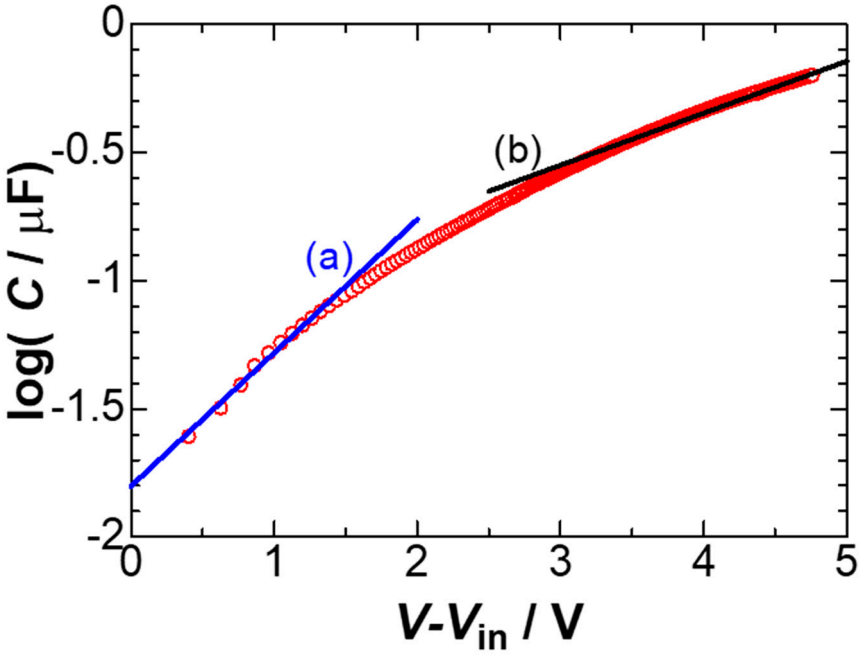

Figure 6. Logarithmic variation of *C* of the supercapacitor in the time domain from 60 s to 90 s with the voltage, $V - V_{in}$. The slopes of the low (a) and the high (b) voltages are 5.0 V^{-1} and 2.0 V^{-1}, respectively.

It is interesting to find where and how the field effect is noticeable in the charging–discharging curves. Combining Equations (2)–(4), we can express the capacitance without any ohmic resistance as

$$C = C_{1s} t^{\lambda} \exp[p(V - V_{in})/k_B T d]. \quad (5)$$

Eliminating C by use of the definition of the charge, $C(V - V_{in}) = jt$, for the constant current density j, we have

$$V - V_{in} = (j/C_{1s})\, t^{1-\lambda} \exp[-p(V - V_{in})/k_B Td], \quad (6)$$

If a value of $p(V - V_{in})/k_B Td$ is close to zero, we can solve Equation (6) approximately with respect to $V - V_{in}$ as

$$V - V_{in} \approx (j/C_{1s})\, t^{1-\lambda}[1 - (j/C_{1s})t^{1-\lambda} p/k_B Td]. \quad (7)$$

This equation indicates that experimentally obtained variations of $V - V_{in}$ vs. t form not a line but a convex represented by ca. $t^{1-\lambda}$ ($\approx t^{0.9}$). The slope of the tangent line is smaller than j/C_{1s}, and it decreases with the time owing to $-(j/C_{1s})t^{1-\lambda} p/k_B Td$. These variations cannot be clearly viewed just by one look of experimental V vs. t curves. We calculated, numerically, Equation (6) with practically employed values of parameters, and plotted $V - V_{in}$ against t in Figure 7 (solid curves). The field effect is revealed as the difference between the dashed curve and the solid curve. It is the convex feature that represents the field effect. Line (a′) is for $\lambda = 0$ or without the power law. This is very close to the dashed curve of the power law. If we take into account only the power law or CPE without the field effect, the power value is estimated to be such a large value ($\lambda = 0.6$), as has been discussed in Figure 5B.

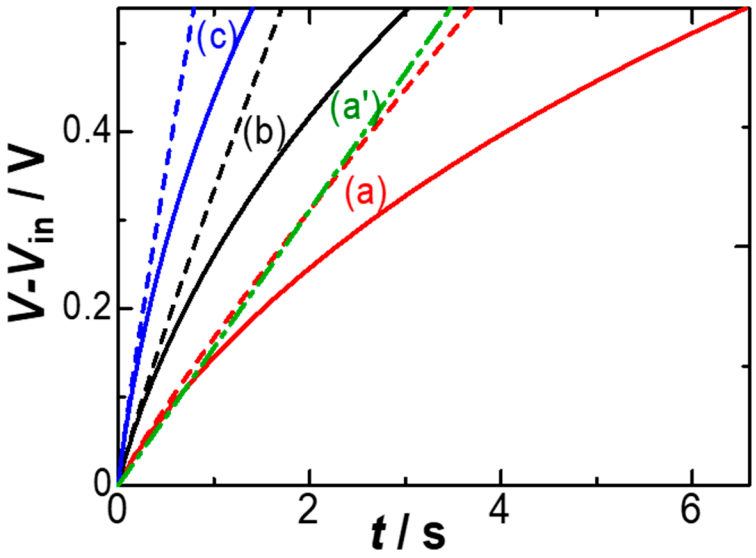

Figure 7. Variations of charging curves calculated from Equation (6) for j = (a) 5, (b) 10, and (c) 20 μA cm^{-2} at C_{1s} = 30 μF cm^{-2}, $\lambda = 0.1$, $p = 1.2 \times 10^{-30}$ Cm, and $d = 0.31$ nm. The dashed curves are for $V - V_{in} = (j/C_{1s})t^{1-\lambda}$ without the field effect. The line (a′) is for $V - V_{in} = (j/C_{1s})t$ (without the power law).

4. Conclusions

The DLC obtained by the constant current-control includes not only the time dependence of the power law but also the field dependence. The latter is much larger than the former for the constant current-control. It is revealed in the convex deviation of the voltage-time curve from the line. It is not noticeable for results by the ac-impedance measurements because the applied voltage is too small to be detected. Since the current-controlled measurement provides voltages as large as 0.3 V, it makes the field effect distinct.

Both effects are included in Equation (5), which is a solution of the kinetic equation for the orientation of interactive dipoles. The field effect is represented in terms of the exponential form of the voltage. The form implies that the voltage can be regarded as a kind of the activation energy of causing the capacitance.

Author Contributions: All authors contributed equally to this manuscript. All authors have read and agreed to the published version of the manuscript.

Funding: This research received no external funding.

Conflicts of Interest: The authors declare no conflict of interest.

References

1. Sivaraman, P.; Thakur, A.; Kushwaha, R.K.; Ratna, D.; Samui, A. Poly (3-methyl thiophene)-activated carbon hybrid supercapacitor based on gel polymer electrolyte. *Electrochem. Solid-State Lett.* **2006**, *9*, A435–A438. [CrossRef]
2. Wang, Q.; Wen, Z.H.; Li, J. A hybrid supercapacitor fabricated with a carbon nanotube cathode and a TiO_2-B nanowire anode. *Adv. Funct. Mater.* **2006**, *16*, 2141–2146. [CrossRef]
3. Rani, J.R.; Thangavel, R.; Oh, S.-I.; Lee, Y.S.; Jang, J.-H. An ultra-high-energy density supercapacitor; fabrication based on thiol-functionalized graphene oxide scrolls. *Nanomaterials* **2019**, *9*, 148. [CrossRef] [PubMed]
4. Wang, F.; Wu, X.; Yuan, X.; Liu, Z.; Zhang, Y.; Fu, L.; Zhu, Y.; Zhou, Q.; Wu, Y.; Huang, W. Latest advances in supercapacitors: From new electrode materials to novel device designs. *Chem. Soc. Rev.* **2017**, *46*, 6816–6854. [CrossRef] [PubMed]
5. Macdonald, J.R. Static space? charge effects in the diffuse double layer. *J. Chem. Phys.* **1954**, *22*, 1317–1322. [CrossRef]
6. Sivaraman, P.; Mishra, S.P.; Potphode, D.D.; Thakur, A.P.; Shashidhara, K.; Samui, A.B.; Bhattacharyya, A.R. A supercapacitor based on longitudinal unzipping of multi-walled carbon nanotubes for high temperature application. *RSC Adv.* **2015**, *5*, 83546–83557. [CrossRef]
7. Kotatha, D.; Hirata, M.; Ogino, M.; Uchida, S.; Ishikawa, M.; Furuike, T.; Tamura, H. Preparation and characterization of electrospun gelatin nanofibers for use as nonaqueous electrolyte in electric double-layer capacitor. *J. Nanotechnol.* **2019**, *2019*, 1–11. [CrossRef]
8. Uchaikin, V.V.; Ambrozevich, A.S.; Sibatov, R.T.; Ambrozevich, S.A.; Morozova, E.V. Memory and nonlinear transport effects in charging–discharging of a supercapacitor. *Tech. Phys.* **2016**, *61*, 250–259. [CrossRef]
9. Lück, J.; Latz, A.; Lueck, J. Modeling of the electrochemical double layer and its impact on intercalation reactions. *Phys. Chem. Chem. Phys.* **2018**, *20*, 27804–27821. [CrossRef]
10. Niu, J.; Pell, W.G.; Conway, B.E. Requirements for performance characterization of C double-layer supercapacitors: Applications to a high specific-area C-cloth material. *J. Power Sources* **2006**, *156*, 725–740. [CrossRef]
11. Singh, A.; Chandra, A. Significant performance enhancement in asymmetric supercapacitors based on metal oxides, carbon nanotubes and neutral aqueous electrolyte. *Sci. Rep.* **2015**, *5*, 15551. [CrossRef] [PubMed]
12. Gu, W.; Solis, M.S.; Magasinski, A.; Fuertes, A.B.; Yushin, G. Sulfur-containing activated carbons with greatly reduced content of bottle neck pores for double-layer capacitors: A case study for pseudocapacitance detection. *Energy Environ. Sci.* **2013**, *6*, 2465. [CrossRef]
13. Allagui, A.; Freeborn, T.J.; Elwakil, A.; Maundy, B.J. Reevaluation of performance of electric double-layer capacitors from constant-current charge/discharge and cyclic voltammetry. *Sci. Rep.* **2016**, *6*, 38568. [CrossRef] [PubMed]
14. Estrada, M.; Ulloa, F.; Ávila, M.; Sanchez, J.; Cerdeira, A.; Castro-Carranza, A.; Iniguez, B.; Marsal, L.F.; Pallares, J. Frequency and voltage dependence of the capacitance of mis structures fabricated with polymeric materials. *IEEE Trans. Electron Devices* **2013**, *60*, 2057–2063. [CrossRef]
15. Ang, C.; Yu, Z. DC electric-field dependence of the dielectric constant in polar dielectrics: Multipolarization mechanism model. *Phys. Rev. B* **2004**, *69*, 174109. [CrossRef]
16. Khaldi, O.; Gonon, P.; Vallée, C.; Mannequin, C.; Kassmi, M.; Sylvestre, A.; Jomni, F. Differences between direct current and alternating current capacitance nonlinearities in high-k dielectrics and their relation to hopping conduction. *J. Appl. Phys.* **2014**, *116*, 84104. [CrossRef]
17. Szewczyk, A.; Sikula, J.; Sedlakova, V.; Majzner, J.; Sedlák, P.; Kuparowitz, T. Voltage dependence of supercapacitor capacitance. *Metrol. Meas. Syst.* **2016**, *23*, 403–411. [CrossRef]

18. Zhu, B.; Liu, W.-J.; Wei, L.; Ding, S.-J. Voltage-dependent capacitance behavior and underlying mechanisms in metal-insulator-metal capacitors with Al_2O_3-ZrO_2-SiO_2 nano-laminates. *J. Phys. D Appl. Phys.* **2016**, *49*, 135106. [CrossRef]
19. Lasia, A. Electrochemical Impedance Spectroscopy and its Applications. In *Modern Aspects of Electrochemistry*; Conway, B.E., Bockris, J.O., White, R.E., Eds.; Kluwer Academic/Plenum Publishers: New York, NY, USA, 1999; Volume 32, pp. 143–248.
20. Nyikos, L.; Pajkossy, T. Fractal dimension and fractional power frequency-dependent impedance of blocking electrodes. *Electrochim. Acta* **1985**, *30*, 1533–1540. [CrossRef]
21. Brug, G.; Eeden, A.V.D.; Sluyters-Rehbach, M.; Sluyters, J. The analysis of electrode impedances complicated by the presence of a constant phase element. *J. Electroanal. Chem. Interfacial Electrochem.* **1984**, *176*, 275–295. [CrossRef]
22. Zoltowski, P. On the electrical capacitance of interfaces exhibiting constant phase element behaviour. *J. Electroanal. Chem.* **1998**, *443*, 149–154. [CrossRef]
23. Hou, Y.; Aoki, K.J.; Chen, J.; Nishiumi, T. Invariance of double layer capacitance to polarized potential in halide solutions. *Univers. J. Chem.* **2013**, *1*, 162–169. [CrossRef]
24. Wang, H.; Aoki, K.J.; Chen, J.; Nishiumi, T.; Zeng, X.; Ma, X. Power law for frequency-dependence of double layer capacitance of graphene flakes. *J. Electroanal. Chem.* **2015**, *741*, 114–119. [CrossRef]
25. Hou, Y.; Aoki, K.J.; Chen, J.; Nishiumi, T. Solvent variables controlling electric double layer capacitance at the metal-solution interface. *J. Phys. Chem. C* **2014**, *118*, 10153–10158. [CrossRef]
26. Zhao, X.; Aoki, K.J.; Chen, J.; Nishiumi, T. Examination of the Gouy-Chapman theory for double layer capacitance in deionized latex suspensions. *RSC Adv.* **2014**, *4*, 63171–63181. [CrossRef]
27. Aoki, K.J. Molecular interaction model for frequency-dependence of double layer capacitors. *Electrochim. Acta* **2016**, *188*, 545–550. [CrossRef]
28. Aoki, K.J.; Chen, J.; Wang, Z. Quantitative relation of the frequency dispersion of double layer capacitances to surface roughness. *Adv. Nanosci. Nanotechnol.* **2018**, *1*, 1–7. [CrossRef]
29. Zhang, S.; Pan, N. Supercapacitors performance evaluation. *Adv. Energy Mater.* **2014**, *5*, 1401401. [CrossRef]
30. Heyd, D.V.; Harrington, D.A. Platinum oxide growth kinetics for cyclic voltammetry. *J. Electroanal. Chem.* **1992**, *335*, 19–31. [CrossRef]
31. Aoki, K.J.; Chen, J.; He, R. Potential step for double-layer capacitances obeying the power law. *ACS Omega* **2020**, *5*, 7497–7502. [CrossRef]